01 Jan 1973

Measurement of Unsteady Flows in Mercury with Hot-Film Anemometers

Charles A. Sleicher

G. B. Lim

MEASUREMENT OF UNSTEADY FLOWS IN MERCURY WITH HOT-FILM ANEMOMETERS

C. A. Sleicher and G. B. Lim
University of Washington
Department of Chemical Engineering
Seattle, Washington 98195

ABSTRACT

The difficulties in making turbulence measurments in liquid metals are discussed briefly. Attention is then focused on the problem of frequency response attenuation of hot-film anemometers by the thermal capacity of the thermal boundary layer near cylindrical sensors. A solution is given to the problem of heat transfer from an infinite cylinder normal to the potential flow of a fluid with a small sinusoidal velocity component. Application of the results to anemometer measurements is discussed. Some preliminary experiments on dynamic calibration are reported, and they are in reasonable agreement with the theory for Peclet numbers less than one.

INTRODUCTION

The measurement of turbulence in liquid metals is beset by difficulties not present with most other fluids. The problems are of two kinds -- handling problems and problems of data interpretation. Handling problems are severe with all liquid metals but are tolerable with mercury and sodium-potassium alloys (NaK) since they are liquids at room temperature. With mercury a prime concern is avoidance of its highly toxic vapor, which is injurious even at room temperature. This problem can be overcome by good ventilation and by keeping the mercury in closed containers or covered with oil or water. Mercury is also troublesome because it attacks (amalgamates with) almost all metals except iron. Thus a minute hole or crack in the quartz coating of a hot-film anemometer will lead to destruction of the film.

NaK alloys do not react with most other metals but they react violently with water and vigorously with oxygen and many halogen-containing compounds. The need to avoid contact with air necessitates procedures with which most experimentalists in turbulence are unaccustomed.

The problems of data interpretation from hot-film anemometers in liquid metals are caused by the high thermal conductivity of the metal. There are three problems of special note -- thermal contact resistance, impaired directional sensitivity, and impaired frequency response.

Thermal contact resistance occurs because impurities that collect on the surface of the sensor have much lower thermal conductivity than the fluid. Hence even a small amount of impurity will alter the response significantly. Such impurities collect on the sensor both during operation and in the process of immersion. The pioneering work on turbulence measurements in the presence of thermal contact resistance is by Sajben (13), and an excellent discussion as well as revealing measurements have been provided by Malcolm (10).

Impaired directional sensitivity and frequency response are caused by the existence of a large thermal boundary layer around the probe. (For convenience we use the term thermal boundary layer to mean that region of the fluid in which the temperature perturbation caused by the heated sensor is

significant, though the layer may be so thick that the usual boundary layer approximations are invalid.) The thermal boundary layer is much larger in liquid metals than in other fluids. As a result the directional sensitivity of a cylindrical sensor will be impaired. The reason for this can be sensed by imagining a short sensor, say L/D = 20, in a liquid metal at low velocity (Peclet number). If the Peclet number were low enough, the thermal boundary layer would be much larger than the sensor. Hence inclining the sensor to the flow would have little effect on the boundary layer shape and on the sensor heat transfer rate. This subject has been studied by Hill and Sleicher (3).

Another effect of the large thermal boundary layer on an anemometer in liquid metals is impaired frequency response. In most fluids the thermal capacity of the boundary layer is small and can be neglected compared to the thermal capacity of the sensor. In liquid metals, however, the reverse prevails. Thus it is the thermal capacity of the boundary layer that usually limits the frequency response of anemometers in liquid metals. In some but by no means all situations, the resulting signal attenuation and phase shift occur at frequencies of interest in turbulence. In the remainder of this paper we present an analysis of the frequency response problem and some preliminary experimental results.

THEORETICAL ANALYSES.

In the discussion that follows we consider only the problem of heat transfer to an infinite cylinder of uniform temperature placed in a Newtonian fluid of uniform upstream temperature and uniform but time dependent upstream velocity. Sensors of other shapes are not considered here.

Steady Flow

At very low Peclet numbers it is well known that the heat transfer rate from an object is insensitive to the details of the flow field near the object. That is, a low Peclet number implies that the thermal boundary layer is larger than the hydrodynamic boundary layer. In the limit $Pe \to 0$, the fraction of the thermal boundary layer occupied by the hydrodynamic layer is vanishingly small and, therefore, inconsequential even in the presence of separation. Thus, for example, in the limit $Pe \to 0$, the equation

$$Nu^* = -2/\ln(\alpha Pe),\ \alpha = .2226\ldots \qquad (1)$$

is the result of both Piercy and Winny (12) for potential flow and of Cole and Roshko (2) for Oseen flow (velocity field approximated everywhere by its free stream value).

The potential flow solution for Pe ranging from zero to infinity is given by Tomotika and Yosinobu (14). This solution shows that the Oseen and potential flow solutions depart significantly from each other as the Peclet number increases above 0.3. The Oseen approximation takes no account of the disturbance to the velocity field by the cylinder; similarly, the potential flow field is not an accurate description of the velocity at any Reynolds number. Which of the two gives the better heat transfer calculation is best determined by experiment. The data of Sajben (13) follow the potential flow solution very well up to a Peclet number of about 1, the limit of Sajben's experiments, and hence for steady flow the potential flow solution is superior to the Oseen solution.

Unsteady Oseen Solution

To analyze the dynamic response of a sensor in a fluctuating flow, the velocity field at infinity is taken to be $U_\infty = \overline{U}(1 + \varepsilon \cos \omega t)$. As in steady flow, a low Peclet number implies that the hydrodynamic boundary layer is insignificantly small in relation to the thermal boundary layer. Hence the Oseen approximation, $U = U_\infty$ everywhere, should be a valid approximation for $Pe \ll 1$, and the range of validity of the result should be about the same as for the steady analysis (Peclet numbers less than about 0.3).

An unsteady Oseen analysis of this problem has been given by us (9), but we had overlooked a similar analysis given earlier by Illingworth (6), and we regret this oversight. The problem and the Oseen approximation set by Illingworth and us are identical. In both analyses the steady part of the solution reduces to Equation 1 in the limit $Pe \to \infty$, in

agreement with Cole & Roshko (2). The results for the unsteady part, however, appear in different form. The two forms may or may not be equivalent, but the numerical results presented from them are similar only for low Peclet number, and the range of frequencies and Peclet number covered is different. At Peclet numbers above about 0.5 and at the higher frequencies, the results differ. At the highest Peclet number used by Illingworth, 1.6, he reports negative phase lag, which we do not find. One observation that gives confidence in the correctness of the numerical evaluation of our equations is that in the limit $\omega \to \infty$, the analytical and numerical results are the same.

Potential Flow Solution

The satisfactory agreement of the steady potential flow solutions with Sajben's data gives hope that an unsteady potential flow analysis will be useful up to Peclet numbers of 1 or possibly higher. For that reason we have undertaken this analysis, which is outlined here with further details given in the Appendix.

The problem is to find the heat rate from a heated cylinder of infinite length and uniform temperature T_w normal to a fluid whose upstream temperature and velocity are T_∞ (constant) and $U_\infty = \bar{U}_\infty (1 + \varepsilon \cos \omega t)$. Potential flow is assumed so that the equation to be solved is, in nondimensional form,

$$\frac{\partial T}{\partial t} + \frac{Pe}{2}\left[U \frac{\partial T}{\partial x} + V \frac{\partial T}{\partial y}\right] = \nabla^2 T \qquad (2)$$

$$U = \left(1 - \frac{1}{r^2} \cos 2\theta\right)(1 + \varepsilon \cos \omega t) \qquad (3a)$$

$$V = \left(-\frac{1}{r^2} \sin 2\theta\right)(1 + \varepsilon \cos \omega t), \qquad (3b)$$

where $T = 1$ at $r = 1$

$T = 0$ at $r = \infty$

As in the previous analysis, we only consider small ε, which permits use of a perturbation method to approximate the solution. Thus the temperature and the heat rate per unit length are taken to be

$$T(r,\theta,t) = T_0(r,\theta) + T_1(r,\theta,t)\,\varepsilon + T_2(r,\theta,t)\varepsilon^2 + \ldots \qquad (4)$$

and

$$Q(t) = Q_0 + Q_1(t)\,\varepsilon + Q_2(t)\,\varepsilon^2 + \ldots \qquad (5)$$

Solutions for the heat rates Q_0 and Q_1, the primary quantities of interest, are given in the Appendix in terms of a rather formidable appearing collection of Mathieu functions. Expressions for these functions, however, are given in Reference 11, which permits numerical results to be achieved without great difficulty on a computer.

RESULTS AND DISCUSSION

The solution for Q_0 is given in the Appendix by Equation A4, which is the same as that obtained by Tomotika and Yosinobu (14). The expression for Q_1, Equation A17, has been evaluated numerically. Before presenting the results, however, it is instructive to consider the asymptotic form of Equation A17 in the limit as $Pe \to 0$. In this case the Mathieu functions can be simplified to

$$\frac{FEK_0(\xi,-\bar{P}^2)}{FEK_0(0,-\bar{P}^2)} = -\frac{K_0(\bar{P}r)}{\ln(\alpha\bar{P})} \qquad (6a)$$

and

$$\frac{FEK_1(\xi,-\bar{P}^2)}{FEK_1(0,-\bar{P}^2)} = \bar{P}\,K_1(\bar{P}r), \qquad (6b)$$

where K_0 and K_1 are modified Bessel functions of zero and first order, and $\alpha = 0.2226$. By substituting Equation 6 into Equation A17, Equation A17 can be simplified to

$$\frac{Q_1}{(T_w - T_\infty)} = \frac{2\pi}{\ln^2(\alpha Pe)} \qquad \text{at } \omega = 0 \qquad (7)$$

This equation is identical to the one obtained for Oseen flow (9) for the same limits, $Pe \to 0$, $\omega = 0$. This finding gives us confidence that our algebra is correct, and it suggests that the unsteady heat flux Q_1 is, like Q_0, insensitive to the velocity field at low Peclet number.

Relations Between $\bar{U}$, u, Q_0, Q_1, and Anemometer Voltages

It is desirable to present the results in a useful form, and for that purpose we now derive the relation between velocity fluctuation and anemometer signal. The rate of heat generation in the sensor is

$$\frac{R}{(R + R^*)^2} (\bar{E} + e)^2 = \frac{R\bar{E}^2}{(R + R^*)^2} (1 + 2 \frac{e}{\bar{E}} + \frac{e^2}{\bar{E}^2}).$$

The rate of heat loss from the sensor is

$$LQ = LQ_0 (1 + \varepsilon \frac{Q_1}{Q_0} + \varepsilon^2 \frac{Q_2}{Q_1} + \ldots)$$

Equating the above expressions and neglecting second-order perturbations yields

$$\frac{R\bar{E}^2}{(R + R^*)^2} (1 + 2 \frac{e}{\bar{E}}) = LQ_0 (1 + \varepsilon \frac{Q_1}{Q_0}). \quad (8)$$

Since the steady and unsteady parts of Equation 8 are separately equal,

$$\frac{R\bar{E}^2}{(R + R^*)^2} = LQ_0 \quad (9)$$

and

$$\frac{2e}{\bar{E}} = \varepsilon \frac{Q_1}{Q_0} \quad (10)$$

Since

$$U = \bar{U} + u = \bar{U} + \bar{u} \cos \omega t = \bar{U} (1 + \varepsilon \cos \omega t),$$

$$e = \frac{1}{2} \bar{E} \frac{\bar{u}}{\bar{U}} \frac{|Q_1|}{Q_0} \cos (\omega t - \phi) \quad (11)$$

$$= \frac{1}{2} \frac{\bar{E}}{\bar{U}} \frac{|Q_1|}{Q_0} \frac{u}{\cos \omega t} \cos (\omega t - \phi)$$

or $$e = \frac{1}{2} \frac{\bar{E}}{\bar{U}} \frac{|Q_1|}{Q_0} (\cos \phi + \sin \phi \tan \omega t)\, u \quad (12)$$

At low frequencies $\phi = 0$ and Equation 12 becomes

$$e = \frac{1}{2} \frac{\bar{E}}{\bar{U}} F_s u = s_s u, \quad (13)$$

where $F_s \equiv |Q_1|_{\omega = 0} / Q_0$ is a static sensitivity factor, and

$$s_s = \frac{1}{2} \frac{\bar{E}}{\bar{U}} F_s$$

is the anemometer static sensitivity. Equation 13 is a statement that the quasi steady-state assumption is valid.

At frequencies high enough that phase shift and attenuation are significant, Equation 12 can be written

$$e = \frac{1}{2} \frac{\bar{E}}{\bar{U}} F_s A (\cos \phi + \sin \phi \tan \omega t)\, u = s_d u, \quad (14)$$

where $A \equiv |Q_1| / |Q_1|_{\omega=0}$ is a normalized dynamic attenuation factor, and s_d is the dynamic sensitivity: $s_d = s_s A (\cos \phi + \sin \phi \sin \omega t)$.

Note that when ϕ is small, to first order in ϕ,

$$e = s_s A (1 + \phi \tan \omega t)\, u. \quad (15)$$

In this case the sensitivity is independent of t except for two brief instants during each cycle of u.

Equation 11 can be used to find a relation between the rms values of e and u, as previously reported in Reference 9:

$$e' = s_s A u' \quad (16)$$

Results

The results of the potential flow analysis are presented in Figures 1-5 and in two tables in the Appendix. Also shown in the figures are curves for the Oseen analysis (9).

Figures 1 and 2 show values of the dynamic attenuation factor A, and the phase angle is shown in Figures 3 and 4. As anticipated, there is a signal attenuation and phase shift at high frequencies, and the difference between Oseen and potential flow is small for Peclet numbers less than about 0.4. Even at Pe = 2, the difference is not large until the dimensionless frequency exceeds unity.

From Figures 1-4 we can find the following useful empirical relations: The frequency at which an anemometer signal is attenuated by 10% (A = 0.9) and at which the phase angle is $\phi = 15°$ are both given approximately by

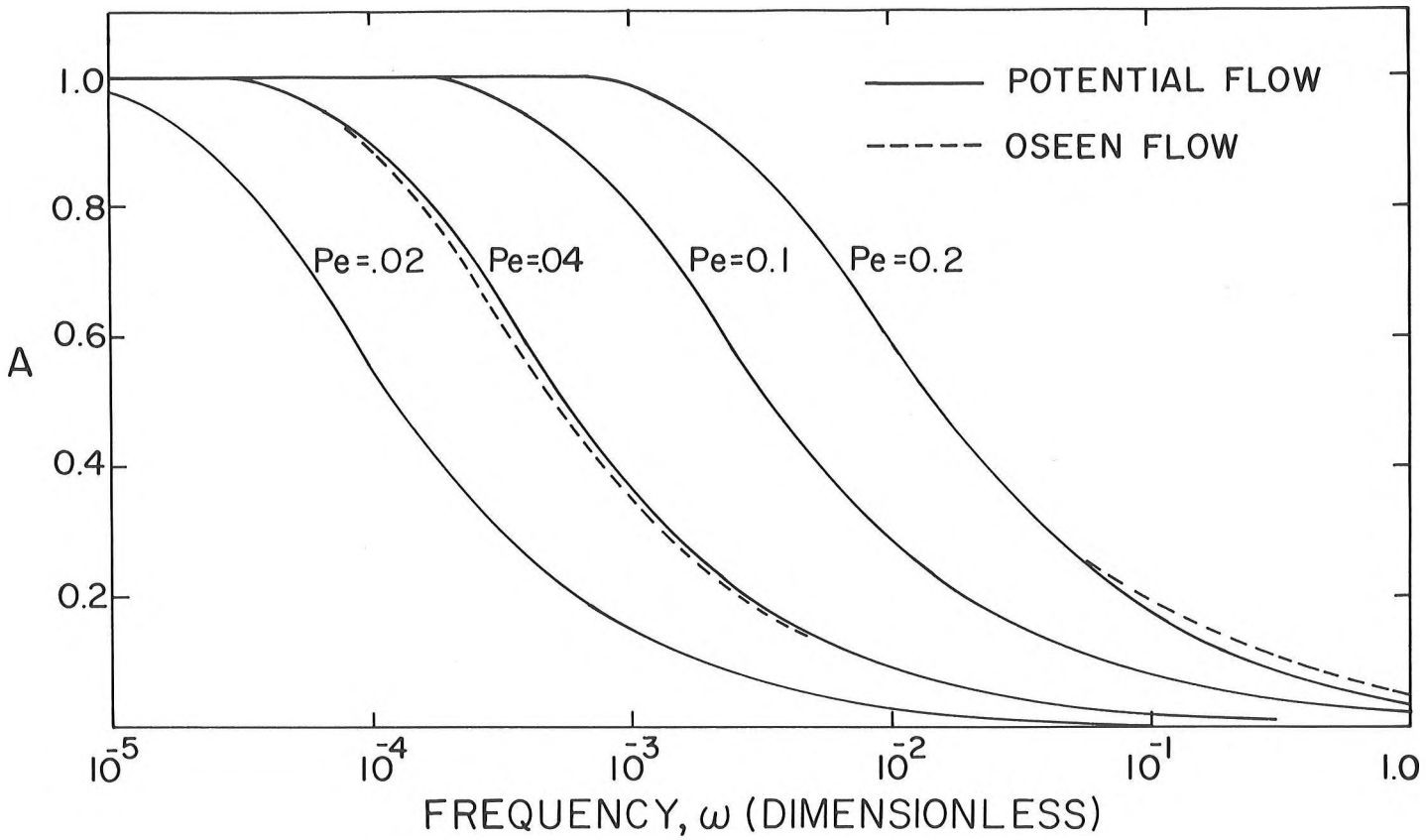

Figure 1. Dynamic Attenuation From Oseen and Potential Flow Analyses

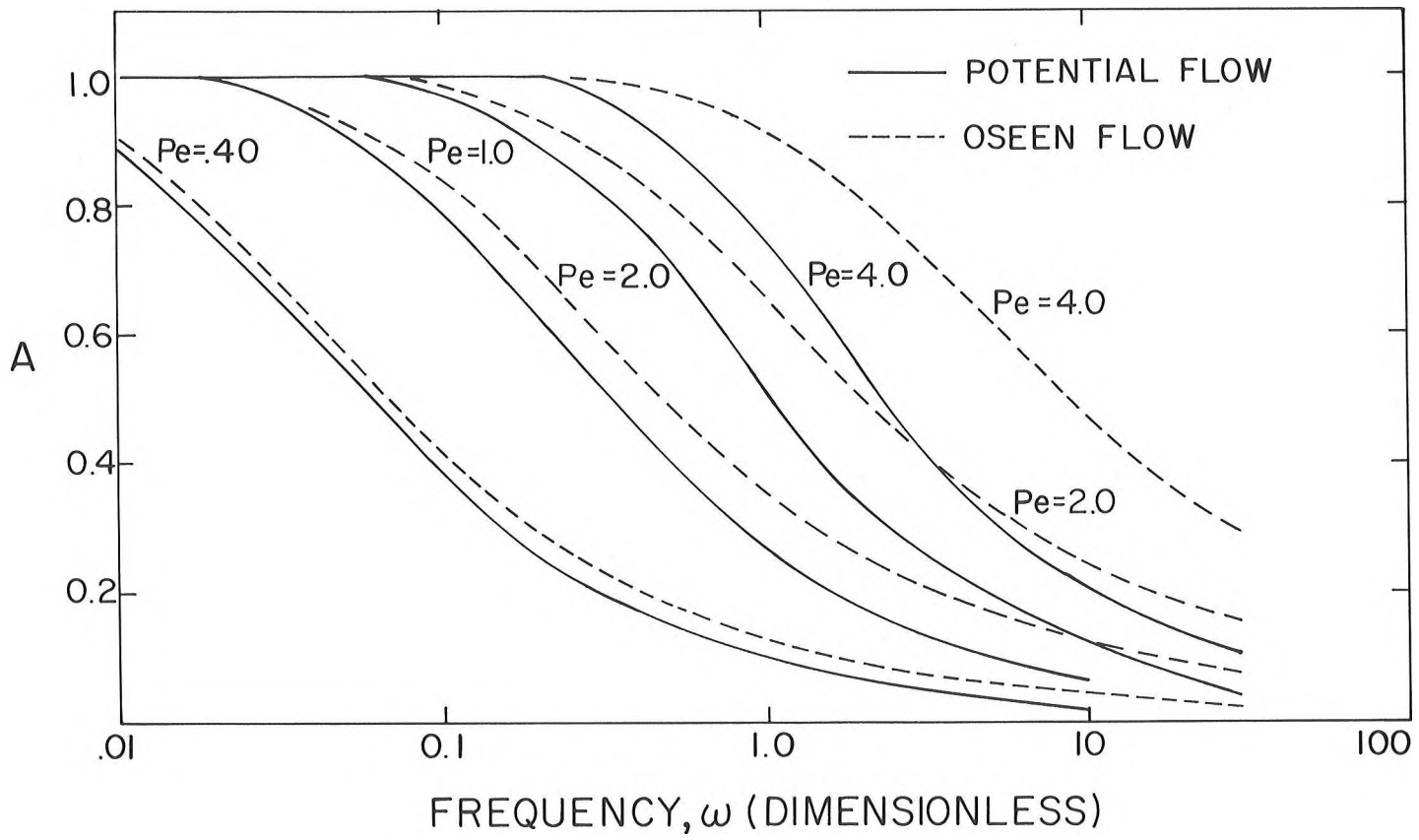

Figure 2. Dynamic Attenuation From Oseen and Potential Flow Analyses

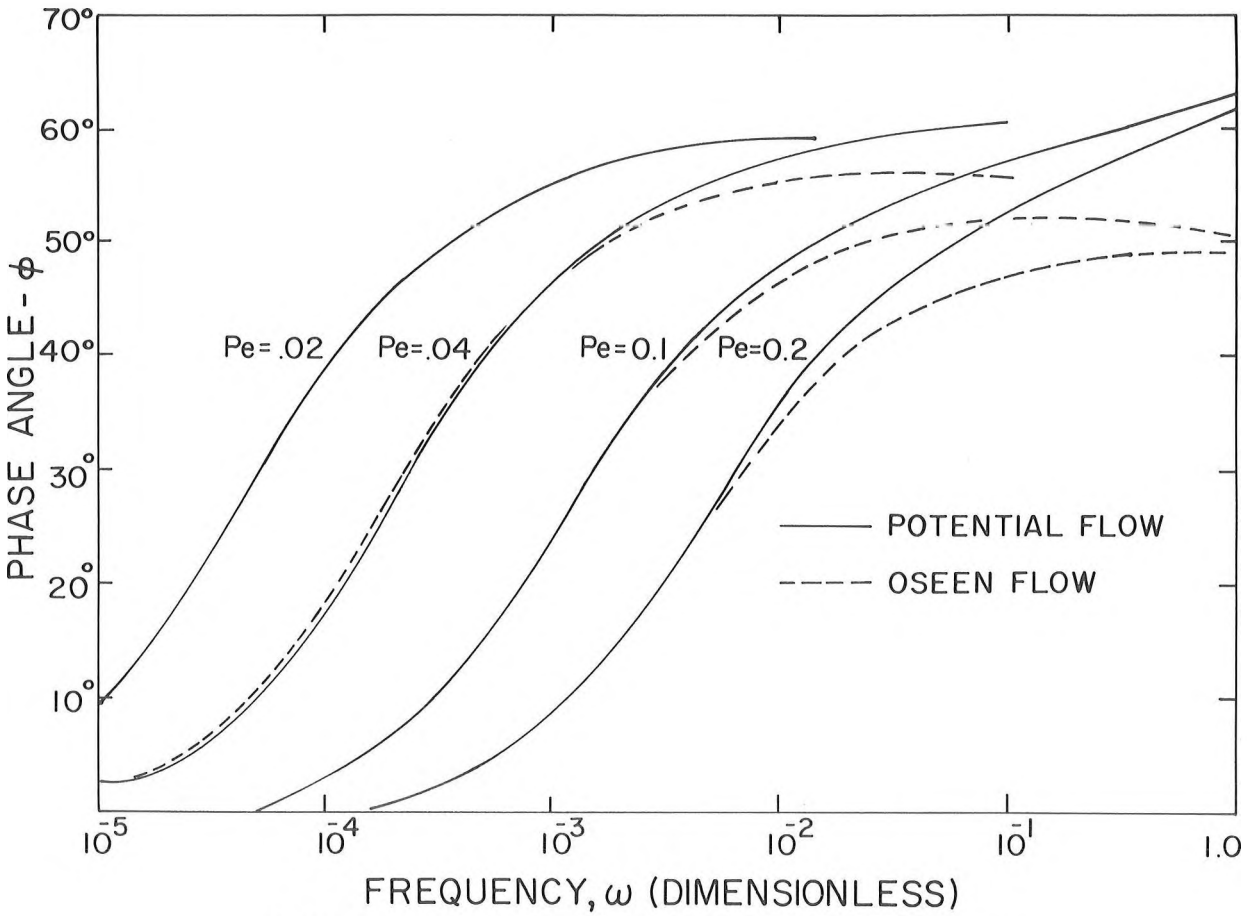

Figure 3. Phase Angle From Oseen and Potential Flow Analyses.

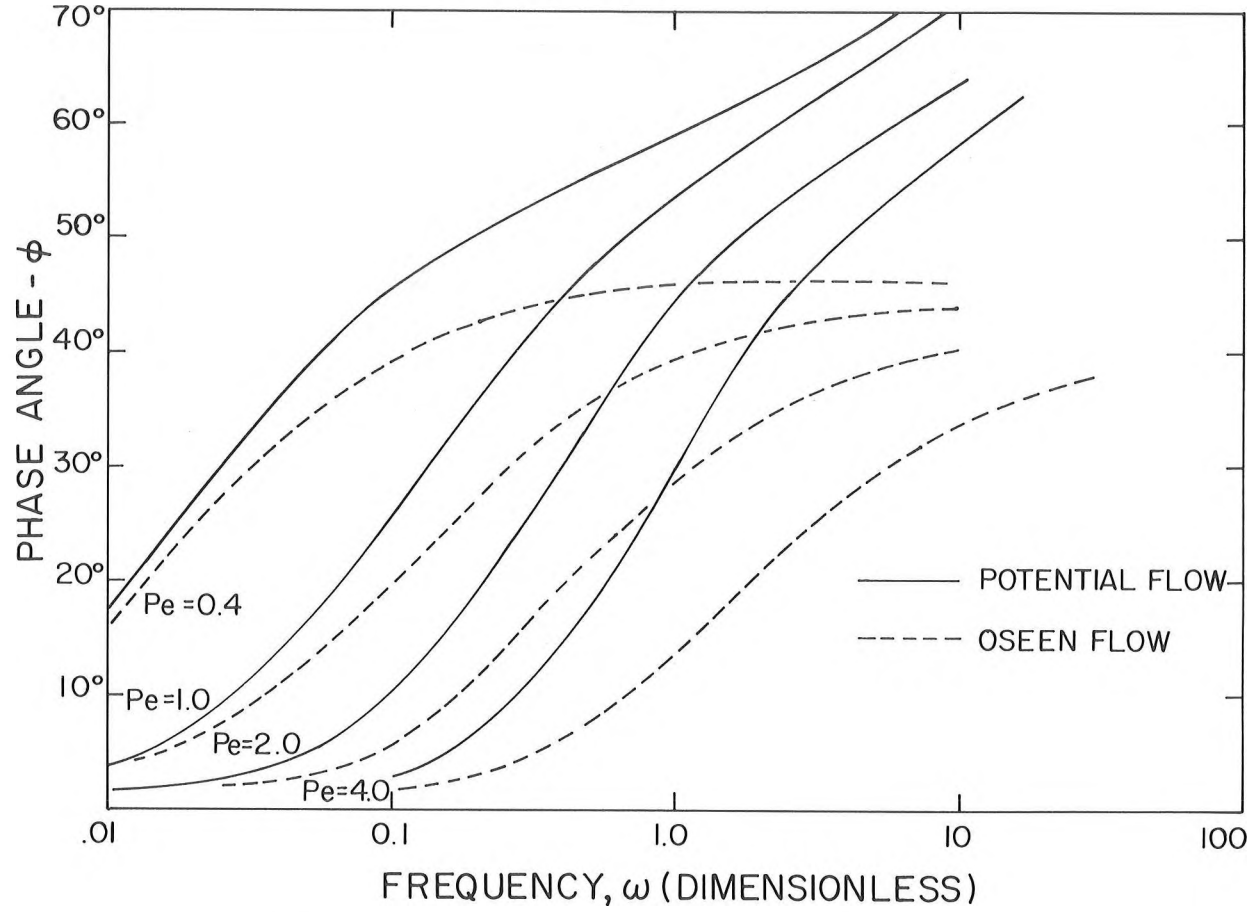

Figure 4. Phase Angle From Oseen and Potential Flow Analyses

$$\omega^*_{(A=.9)} = \omega^*_{(\phi=15)} = .032\ \bar{U}^2/\kappa. \qquad (17)$$

This equation should be useful for the purpose of determining when a dynamic calibration or correction is needed.

Figure 5 shows values of the static sensitivity factor F_s. The curves for Oseen and potential flow are calculated from the theories described. It is useful to note, however, that such curves can also be obtained from a static calibration of a probe. To obtain F_s from an experimental plot of Nu vs Pe, one writes

$$Nu = \frac{Q}{\pi LK\Delta T} = \frac{RE^2}{\pi Lk\Delta T(R+R^*)^2}$$

$$Pe = \frac{D\rho C_p}{k} U$$

so that $$\frac{dNu}{dPe} = 2\,\frac{Nu}{Pe}\,\frac{U}{E}\,\frac{dE}{dU}.$$

But dE = e and dU = u, and with Equation 13

$$\frac{dNu}{dPe} = 2\,\frac{Nu}{Pe}\,\frac{1}{2}F_s$$

or

$$\frac{d\ \ln\ Nu}{d\ \ln\ Pe} = F_s. \qquad (18)$$

To illustrate the use of this equation and to verify the computations of $|Q_1|_{\omega=0}$, we have used Equation 18 to calculate F_s from

$$Nu = \frac{1 + 2.03Pe^2}{2Pe^{3/2} - \frac{1}{2}\ln(\alpha Pe)}, \qquad (19)$$

which is given by Hill and Sleicher (4) as a correlation of the potential flow calculations of Tomotika and Yosinobu (14). As shown in Figure 5, the agreement between the two methods of calculating F_s is satisfactory.

Frequencies of Applicability

To determine whether or not frequency attenuation and phase shift occur at frequencies of interest, we can compare the frequency given by Equation 17 to the frequency at the maximum of the energy spectrum, ω^*_e, and to the frequency at the Kolmogoroff wave number, ω^*_k.

There are two ways in which we have derived expressions for the frequency of the "energy-containing eddies" in a pipe. Using expressions in Hinze (5), we find

$$\omega^*_e = \frac{k_e\bar{U}}{2\pi} = \frac{\bar{U}}{2\pi}\,\frac{E}{\bar{A}\,u'^3}$$

where $\bar{A}$ is a constant of order unity.

Now let $W_o = ED/2u^{*3}$, a dimensionless energy dissipation rate.

Then $$\omega^*_e = \frac{\bar{U}}{\pi\,\bar{A}D}\left(\frac{u^{*3}}{u'^3}\right) W_o$$

Combining this equation with Equation 17, we relate $\omega^*_{A=.9}$ to ω^*_e:

$$\frac{\omega^*_{A=.9}}{\omega^*_e} = 0.10\,\bar{A}\,Pe\,\left(\frac{u'}{u^*}\right)^3\frac{1}{W_o} \qquad (20)$$

Near a pipe center Laufer (7) finds $u'/u^* = 0.8$ and $W_o \approx 2.5$. Then with $\bar{A} = 1$,

$$\frac{\omega^*_{A=.9}}{\omega^*_e} = 0.02\ Pe \quad \text{at pipe center.} \qquad (21)$$

Alternatively, Baldwin and Walsh (1) have measured the Lagrangian integral scale Λ in a pipe center and find approximately $\Lambda = 0.035D$. The integral scale should correspond roughly to the size of the energy containing eddies, so

$$\omega^*_e = \frac{\bar{U}}{\Lambda} \approx \frac{\bar{U}}{.035}$$

With Equation 17 the above equation gives

$$\frac{\omega^*_{A=.9}}{\omega^*_e} = 0.001\ Pe. \qquad (22)$$

Though not the same, Equations 21 and 22 are in sufficient agreement for our purposes. Probably Equation 22 is better, for its derivation is more direct.

The Kolmogoroff wave number is $k_k = (E/\nu^3)^{1/4}$, or

$$\omega^*_k = \frac{k_k\bar{U}}{2\pi} = \frac{\bar{U}}{2\pi}\left(\frac{E}{\nu^3}\right)^{1/4} = \frac{\bar{U}}{2\pi}\left(\frac{2u^{*3}W_o}{D\nu^3}\right)^{1/4} \qquad (23)$$

Using Equations 17 and 23, the definition of u*, and the Blasius expression for the friction factor

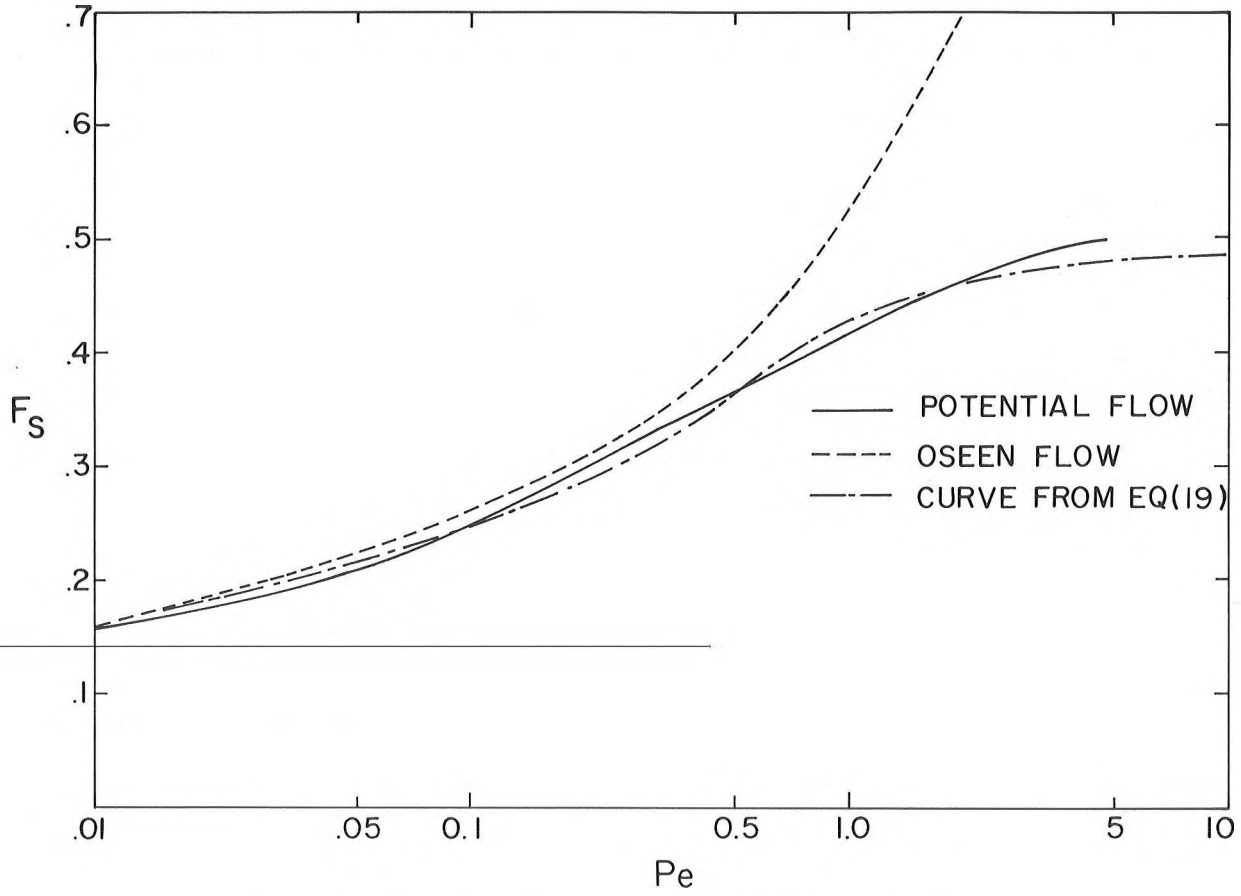

Figure 5. Static Sensitivity Factor For Oseen and Potential Flow

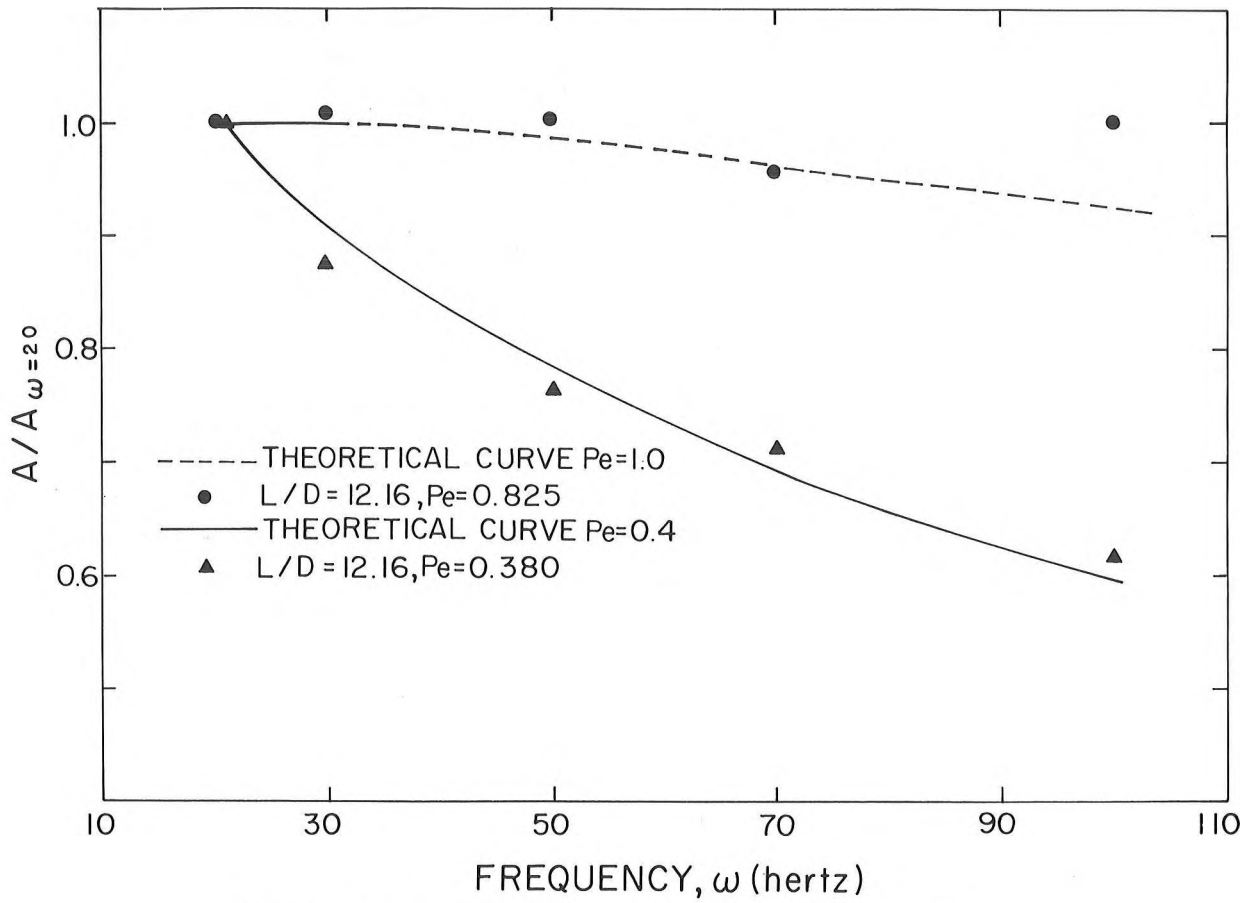

Figure 6. Comparison of Calculated Attenuation to Preliminary Experiments

$$f = .316\ Re^{-.25},$$

we find

$$\frac{\omega^*_{A=.9}}{\omega^*_k} = .26\ \frac{\bar{U}}{U_{ave}}\ W_o^{-.25}\ Pr\ Re^{.34} \qquad (24)$$

At a pipe center $W_o \approx 2.5$ and the above equation yields

$$\frac{\omega^*_{A=.9}}{\omega^*_k} = .17\ Pr\ Re^{.34} \qquad (25)$$

with smaller values at other radii.

For illustration, let us now apply Equations 22 and 25 to two cases. For mercury ($Pr \approx .025$) at $Re = 50{,}000$ we find $\omega^*_{A=.9}/\omega^*_e = 2.5$ and $\omega^*_{A=.9}/\omega^*_k = 0.21$, i.e., the attenuation frequency exceeds ω^*_e by a factor of 2.5 but is smaller than the Kolmogoroff frequency by a factor of about 5. In this case most of the frequencies of interest cause anemometer attenuation. For a second example take $N_a K$ ($Pr \approx .01$) at $Re = 100{,}000$. Then $\omega^*_{A=.9}/\omega^*_e = \omega^*_{A=.9}/\omega^*_k = 0.09$. In this case and at all lower Reynolds numbers all the frequencies of interest will be attenuated.

Some Preliminary Experimental Results

Some dynamic calibrations have been made in a trough of mercury 4.9 m long, 5 cm wide, and 5 cm deep. The probe was a quartz-coated cylindrical film probe of L/D = 12 made by Thermo-Systems, Inc., and driven by a Thermo-Systems 1010 anemometer. The probe was towed normal to its axis and was oscillated parallel to its mean velocity by a loudspeaker. The probe support mechanism and loudspeaker were mounted on a cart which rolled on two parallel polished steel rods beside and physically detached from the trough. Noise in the appartus was kept low by the use of instrument quality ball bearings. The data were recorded on magnetic tape, digitized, and analyzed for frequency content by fast Fourier transform on a CDC 6400 computer. With the probe not oscillating, system noise appeared to be random except for a weak peak at about 340 Hertz, which apparently corresponded to some natural frequency of the system. In the experiment reported here the signal-to-noise ratio was of order 100, and the highest oscillation frequency was 100.

Figure 6 shows the amplitude attenuation factor A normalized by its value at $\omega^* = 20$ Hz. It would be preferable, of course, to normalize A with its value at $\omega^* = 0$, i.e., unity, but we were unable to obtain a frequency below 20 Hz in the experiment. The attenuation is in satisfactory agreement with experiment. Indeed, the agreement is surprising in view of the short aspect ratio. This gives us some hope that the analysis presented here will lessen or possibly eliminate the need for a dynamic calibration.

The following scheme is tentatively posed as a substitute for a dynamic calibration. First, a careful static calibration must be made. Then values of F_s can be prepared from this calibration by Equation 18. The dynamic response is then given by Equation 14 or 15.

The rationale for this procedure is the hope that the attenuation factor A is independent of the quartz coating and surface impurities and is, perhaps, only weakly dependent on L/D, ε, and the presence of the probe supports. On the other hand, F_s is strongly dependent on geometry and surface conditions and so must be determined from experiment.

CONCLUSIONS

The dynamic response of a hot-film anemometer in liquid metals is shown to be significantly attenuated by the thermal capacity of the liquid in the frequency range of practical interest. Therefore, the usual quasi-steady state calibration, $e = s_s u$, is invalid at high frequencies. The frequencies above which the quasi-steady state assumption is invalid can be estimated from Equation 17:

$$\omega^*_{A=.9} = 0.032\ \bar{U}^2/\kappa$$

At frequencies higher than this value a dynamic calibration is necessary.

In the absence of a dynamic calibration a procedure preferable to the quasi-state assumption is to use $e = s_d u$. The dynamic sensitivity, s_d, is then related to the static sensitivity by

$s_d = s_s A(\cos\phi + \sin\phi \sin \omega t)$ where A and ϕ are functions of frequency and Peclet number presented in this paper.

ACKNOWLEDGMENT

The authors are grateful to the National Science Foundation for the support of this study.

SYMBOLS

A	$\lvert Q_1\rvert / \lvert Q_1\rvert_{\omega=0}$, dynamic attenuation factor
C_p	specific heat
D	probe or pipe diameter
E	anemometer voltage, $E = \bar{E} + e$
$\bar{E}$	steady component of E
$\mathcal{E}$	energy dissipation rate
e'	rms value of e
e	unsteady component of e
f	Moody friction factor
F_s	$\lvert Q_1\rvert_{\omega=0}/Q_0$, static sensitivity factor
k	thermal conductivity or wave number
k_k	Kolmogoroff wave number, $(\mathcal{E}/\nu^3)^{1/4}$
L	sensor length
Nu	Nusselt number based on hot film temperature
Nu*	Nusselt number based on sensor surface temperature
$\bar{P}$	Pe/4
Pe	Re Pr, Peclet number
Pr	ν/κ, Prandtl number
Q	heat rate per unit sensor length
R	sensor resistance
R*	lead and bridge resistance in series with sensor
Re	Reynolds number DU_{ave}/ν (pipe), $D\bar{U}/\nu$ (cylinder)
r	dimensionless radial variable
r_o	cylinder radius
s	$s^2 = i\omega + \bar{P}^2$
s_d	dynamic anemometer sensitivity
s_s	static anemometer sensitivity
T	temperature
t	dimensionless time, $t = t^* \kappa/r_o^2$
U	x-component of velocity, $U = \bar{U} + u$
$\bar{U}$	steady part of U
U_{ave}	bulk-average velocity in a pipe
u	unsteady part of U
$\bar{u}$	amplitude of velocity fluctuation, $u = \bar{u} \cos \omega t$
u^*	friction velocity, $U_{ave}\sqrt{f/8} = \sqrt{\tau_w/\rho}$
u'	rms value of u
V	y component of velocity
x,y	rectangular coordinate variables
α	0.2226....
ε	perturbation parameter
η	$\xi = \eta + \ln\sqrt{P/s}$
θ	cylindrical coordinate angle
κ	thermal diffusivity
ν	kinematic viscosity
ξ	ln r
ρ	density
ϕ	phase angle between U_∞ and Q_1
ω	dimensionless frequency, $\omega = 2\pi\, \omega^* r_o^2/\kappa$
ω^*	frequency, Hz
ω_e^*	frequency of maximum of energy spectrum
ω_k^*	Kolmogoroff frequency

Subscripts

w	at wall (or surface)
∞	at infinity

0,1,2 order of perturbations of T and Q

REFERENCES

1. L. V. Baldwin and T. J. Walsh, Turbulent Diffusion in the Core of Fully-Developed Pipe Flow, A.I.Ch.E. J., 7, 53-61 (1961).

2. J. Cole and A. Roshko, Heat Transfer From Wires at Reynolds Numbers in the Oseen Range, Proc. Heat Transf. Fluid Mech. Inst., pp. 13-25. University of California, Berkeley (1954).

3. J. C. Hill and C. A. Sleicher, Directional Sensitivity of Hot-Film Sensors in Liquid Metals, Rev. Sci. Instr. 42, 1461-1468 (1971).

4. J. C. Hill and C. A. Sleicher, Convective Heat Transfer From Small Cylinders to Mercury, Int. J. Heat Mass Transfer, 12, 1595-1604 (1969).

5. J. O. Hinze, Turbulence, McGraw-Hill Book Co., New York (1959), p. 182-201.

6. C. R. Illingworth, A note on fluctuating heat transfer at small Peclet numbers, J. Fluid Mech., 7, 442-448 (1960).

7. J. Laufer, The Structure of Turbulence in Fully Developed Pipe Flow, NACA TR 1174 (1954).

8. G. B. Lim, Dynamic Response of Hot Film Anemometers in Liquid Metals, Ph.D. Dissertation, Dept. of Chem. Eng., Univ. of Washington (1973).

9. G. B. Lim and C. A. Sleicher, The Dynamic Behavior of Hot-Film Anemometers in Liquid Metals, Flow: Its Measurement and Control in Science and Industry, Vol. I, Part 2, 563-570, Instrument Soc. of America, Pittsburgh, Pa. (1974).

10. D. G. Malcolm, Some Aspects of Turbulence Measurement in Liquid Mercury Using Cylindrical Quartz-Insulated Hot-Film Sensors, J. Fluid Mech., 37, 701-714 (1969).

11. N. W. McLachlan, Theory and Application of Mathieu Functions, Oxford U. Press (1947), p. 248.

12. N. A. V. Piercy and H. F. Winny, The Convection of Heat From Isolated Plates and Cylinders in an Inviscid Stream, Phil. Mag., 16 (7), 390-408 (1933).

13. M. Sajben, Hot-Wire Anemometry in Liquid Mercury, Rev. Sci. Instr., 36, 945-949 (1965).

14. S. Tomotika and H. Yosinobu, On the Convection of Heat From Cylinders Immersed in a Low-speed of Incompressible Fluid, J. Math. Phys., 36, 112-120 (1957).

APPENDIX

Here we outline the steps in the solutions of Equations 2 and 4 for T_0 and T_1 and the corresponding heat rates Q_0 and Q_1. Details of the solution are given by Lim (8).

Equation 2 can be rearranged to

$$\frac{\partial T}{\partial t} + 2\bar{P}\,(1+\varepsilon\cos\omega t)\left[\left(1-\frac{1}{r^2}\right)\cos\theta\,\frac{\partial T}{\partial r}\right. \quad \text{(A1)}$$

$$\left. -\frac{\sin\theta}{r}\left(\frac{1}{r^2}+1\right)\frac{\partial T}{\partial\theta}\right] = \nabla^2 T$$

Now let $\xi = \ln r$. (This simple coordinate transformation transforms the steady part of (A1) into the same form obtained by Tomotika and Yosinobu (14) through the use of Boussinesq's transformation.) Then (A1) becomes

$$e^{2\xi}\frac{\partial T}{\partial t} + 4\bar{P}(1+\varepsilon\cos\omega t)\left(\sinh\xi\cos\theta\right. \quad \text{(A2)}$$

$$\left.\frac{\partial T}{\partial\xi} - \sin\xi\cosh\xi\frac{\partial T}{\partial\theta}\right) = \frac{\partial^2 T}{\partial\xi^2} + \frac{\partial^2 T}{\partial\theta^2}$$

$$\text{Let } T = T_0(r,\theta) + \varepsilon\, T_1(r,\theta,t) + \ldots, \quad \text{(A3)}$$

put (A3) into (A2) and collect terms having the same order in ε.

Solution for T_0 and Q_0

The solution for Q_0 has been given by Tomotika and Yosinobu. From their Equation 5.4, we find

$$-\frac{Q_0}{k(T_w-T_\infty)} = \sum_{m=0}^{\infty} B_m \quad \text{(A4)}$$

$$B_{2m} = -\frac{4\pi[ce_{2m}(0,-\bar{P}^2)]^2 A_0^{(2m)}}{FEK_{2m}(0,-\bar{P}^2)\,ce_{2m}(0,\bar{P}^2)}$$

$$B_{2m+1} = \frac{4\pi[ce_{2m+1}(0,-\bar{P}^2)]^2\bar{P}\,B_1^{(2m+1)}}{FEK_{2m+1}(0,\bar{P}^2)\,se'_{2m+1}(0,\bar{P}^2)}$$

where $ce_{2m}(\theta,\bar{P}^2)$ and $se_{2m+1}(\theta,-\bar{P}^2)$ are Mathieu functions, and $FEK_{2m+1}(\xi,-\bar{P}^2)$ and $FEK_{2m}(\xi,-\bar{P}^2)$ are modified Mathieu functions. Expressions for these Mathieu functions are given in Reference (11).

Solution for T_1 and Q_1

The equation for T_1 is

$$e^{2\xi}\frac{\partial T_1}{\partial t} + 4\bar{P}\left[\sinh\xi\cos\theta\,\frac{\partial T_1}{\partial\xi} - \sin\theta\cosh\xi\right.$$

$$\left.\frac{\partial T_1}{\partial\theta}\right] = \nabla^2 T_1 - \cos\omega t\,\nabla^2 T_0$$

$$T_1(0,\theta,t) = T_1(\infty,\theta,t) = 0$$

Put $T_1 = \phi_1(\xi,\theta)\exp(i\omega t + 2\bar{P}\cos\theta\cosh\xi)$ into (A5) and obtain

$$\phi_1[i\omega e^{2\xi} + 2\bar{P}^2\cosh 2\xi - 2\bar{P}^2\cos 2\theta] =$$

$$\nabla^2\phi_1 - e^{2\bar{P}\cosh\xi\cos\theta}\nabla^2 T_0$$

Now let

$$\phi_1 = \sum_{n=0}^{\infty} R_n(\xi)\,\psi(\theta) \quad \text{(A7)}$$

where $\psi(\theta)$ is found to be $ce_n(\theta,-\bar{P}^2)$, a Mathieu function satisfying

$$\frac{d^2 ce_n}{d\theta^2} + [\alpha_n + 2\bar{P}^2\cos 2\theta]ce_n = 0$$

Put (A7) into (A6) and with $s^2 = i\omega + \bar{P}^2$ and obtain

$$\frac{d^2R_n}{d\xi^2} - [\alpha_n + s^2e^{2\xi} + \bar{P}^2 e^{-2\xi}]R_n = H_n(\xi) \quad (A8)$$

$$H_n(\xi) = \frac{1}{\pi} \int_0^{2\pi} e^{-2\bar{P}\cosh\xi\cos\theta} \nabla^2 T_0(\xi,0)$$

$$ce_n(\theta,-\bar{P}^2)d\theta \quad (A9)$$

Let $\xi=\eta + \ln \sqrt{\bar{P}/s}$ so that

$$e^{2\xi} = e^{2\eta}\,\bar{P}/s$$

$$e^{-2\xi} = e^{-2\eta}s/\bar{P}$$

Substituting these values into (A8) we obtain

$$\frac{d^2R_n}{d\eta^2} - (\alpha_n + 2\bar{P}s\cosh 2\eta)\,R_n = H_n(\xi) \quad (A10)$$

The homogeneous solutions for R_n are modified Mathieu functions. After finding the homogeneous and particular solutions and applying the boundary conditions, we find

$$T_1(\eta,\theta) = e^{i\omega t}\, e^{2\bar{P}\cos\theta\cosh\xi} \sum_{n=0}^{\infty} ce_n(\theta,-\bar{P}^2)R_n(\eta, -s\bar{P}) \quad (A11)$$

with

$$R_n(\eta,-s\bar{P}) = \text{const.}\,[CE_n(\eta,s\bar{P}) \int_{\infty}^{\eta} FEK_nH_nd\eta - FEK_n(\eta,-s\bar{P}) \int_{\eta_o}^{\eta} CE_nH_nd\eta - \frac{FEK_n(\eta,-s\bar{P})CE_n(\eta_o,-s\bar{P})}{FEK_n(\eta_o,-s\bar{P})} \int_{\infty}^{\eta} FEK_nH_nd\eta\,] \quad (A12)$$

where $\eta_o = \ln \sqrt{s/\bar{P}}$.

To obtain Q_1, we have

$$Q_1 = -k(T_w-T_\infty) \int_0^{2\pi} \left(\frac{\partial T_1}{\partial\eta}\right)_{\eta_o} d\theta \quad (A13)$$

Put T_1 from (A11) into (A13) and make use of Equation 5.5 of Tomotika and Yosinobu:

$$\int_0^{2\pi} e^{2\bar{P}\cos\theta}\, ce_n(\theta,-\bar{P}^2)\,d\theta = C_n \quad (A14)$$

where C_n is given in Tomotika's paper. We then find

$$-\frac{Q_1}{k(T_2 - T_\infty)} = e^{i\omega t} \sum_{n=o}^{\infty} C_n \left(\frac{dR_n}{d\eta}\right)_{\eta=\eta_o} \quad (A15)$$

The derivative is found from (A11), which after some manipulation gives

$$\left(\frac{dR_n}{d\eta}\right)_{\eta=\eta_o} = \frac{1}{FEK_n(\eta_o,-s\bar{P})} \int_{\infty}^{\eta_o} FEK_nH_nd\eta \quad (A16)$$

The problem is now reduced to Equations A15 and A16 with H_n given by Equation A9. These equations can be simplified with trigonometric identities, and the final result is

$$-\frac{Q_1}{k(T_w-T_\infty)} = e^{i\omega t} \sum_{n,m=0}^{\infty} Q_{n,m} \quad (A17)$$

$$Q_{n,m} = 4\bar{P}\,C_n\,A_m[F_{n,m}E1_{n,m} - G_{n,m}E2_{n,m} + \bar{P}(\delta_m^n E3_{n,m} - D_{n,m}E4_{n,m})] \quad (A17a)$$

where

$$A_{2m} = \frac{2A_0^{(2m)}\, ce_{2m}(0,-\bar{P}^2)}{ce_{2m}(0,\bar{P}^2)} \quad (A17b)$$

$$A_{2m+1} = \frac{2B_1^{(2m+1)}\,\bar{P}\, ce_{2m+1}(0,-\bar{P}^2)}{se'_{2m+1}(0,\bar{P}^2)} \quad (A17c)$$

$$C_{2n} = \frac{2\pi\, ce_{2n}(0,\bar{P}^2\, A_0^{(2n)}}{ce_{2n}(0,\bar{P}^2)} \quad (A17d)$$

$$C_{2n+1} = \frac{2\pi\, ce_{2n+1}(0,-\bar{P}^2)\ \bar{P}\ B_1^{(2n+1)}}{se'_{2n+1}(0,\bar{P}^2)} \qquad \text{(A17e)}$$

$$E1_{n,m} = \int_{\infty}^{\eta_o} \sinh\xi \frac{FEK'_m(\xi,-\bar{P}^2)}{FEK_m(0,-\bar{P}^2)}$$

$$\frac{FEK_n(\eta,-s\bar{P})}{FEK_n(\eta_o,-s\bar{P})}\, d\eta \qquad \text{(A17f)}$$

$$E2_{n,m} = \int_{\infty}^{\eta_o} \cosh\xi \frac{FEK_m(\xi,-\bar{P}^2)}{FEK_m(0,-\bar{P}^2)}$$

$$\frac{FEK_n(\eta,-s\bar{P})}{FEK_n(\eta_o,-s\bar{P})}\, d\eta \qquad \text{(A17g)}$$

$$E3_{n,m} = \int_{\infty}^{\eta_o} \cosh 2\xi \frac{FEK_m(\xi,-\bar{P}^2)}{FEK_m(0,-\bar{P}^2)}$$

$$\frac{FEK_n(\eta,-s\bar{P})}{FEK_n(\eta_o,-s\bar{P})}\, d\eta \qquad \text{(A17h)}$$

$$E4_{n,m} = \int_{\infty}^{\eta_o} \frac{FEK_m(\eta,-\bar{P}^2)}{FEK_m(0,-\bar{P}^2)} \frac{FEK_n(\eta,-s\bar{P})}{FEK_n(\eta,-sP)} d\eta \qquad \text{(A17i)}$$

$\eta_o = \ln\sqrt{s/\bar{P}}$, $s^2 = (i\omega + \bar{P}^2)$, $\xi = \ln r$, $\eta = \xi + \eta_o$

$$F_{n,m} = \frac{1}{\pi}\int_0^{2\pi} \cos\theta\, ce_m(\theta,-\bar{P}^2)\, ce_n(\theta,-\bar{P}^2)\, d\theta \qquad \text{(A17j)}$$

$$G_{n,m} = \frac{1}{\pi}\int_0^{2\pi} \sin\theta\, ce'_m(\theta,-\bar{P}^2)\, ce_n(\theta,-P^2)\, d\theta \qquad \text{(A17k)}$$

$$D_{n,m} = \frac{1}{\pi}\int_0^{2\pi} \cos 2\theta\, ce_n(\theta,-\bar{P}^2)\, ce_m(\theta,-\bar{P}^2)\, d\theta \qquad \text{(A17m)}$$

and $\delta_m^n = 1 \quad n = m$

$\delta_m^n = 0 \quad n \neq m$

The above Mathieu functions can be expressed in terms of Bessel functions so that the problem has been reduced to the evaluation of integrals for which the integrands are calculated from available subroutines. One computer run (given $\bar{P}$, about 10 frequencies) consumed about 60-120 seconds on a CDC 6400.

Table I

$F_s \equiv [|Q_1|/Q_0]_{\omega=0}$ from Potential Flow, Oseen Flow, and Equation 19

Pe	Potential Flow	Oseen Flow	Eqn. (19)
.02	.184	.185	.183
.04	.200	.211	.207
0.1	.253	.260	.246
0.2	.299	.311	.284
0.4	.349	.381	.339
1.0	.412	.518	.431
2.0	.441	.700	.463
4.0	.487	1.17	.477

Table IIa

Fractional Attenuation, $A \equiv |Q_1|/|Q_1|_{\omega=0}$, and Phase Angle ($-\phi$, in Degrees) from Potential Flow Heat Response

ω	Pe=0.02		Pe=0.04		Pe=0.10		Pe=0.20	
	A	$-\phi$	A	$-\phi$	A	ϕ	A	ϕ
1×10^{-6}	1.0	.935	1.0		1.0		1.0	
3×10^{-6}	.998	2.80	1.0		1.0		1.0	
1×10^{-5}	.975	9.02	.999	2.03	1.0		1.0	
3×10^{-5}	.851	22.2	.989	5.99	1.0		1.0	
1×10^{-4}	.560	40.1	.905	17.4	.996	3.34	1.0	
3×10^{-4}	.308	49.2	.671	33.2	.970	9.62	.998	2.52
1×10^{-3}	.148	55.8	.372	46.8	.812	24.3	.978	8.15
3×10^{-3}	.0723	58.2	.195	53.1	.537	38.6	.867	20.2
1×10^{-2}	.0321	59.9	.0912	57.0	.287	43.3	.585	35.9
3×10^{-2}	.0156	58.8	.0445	58.9	.151	53.5	.342	45.9
1×10^{-1}	.00688	58.8	.0200	60.3	.0710	57.1	.172	52.8
3×10^{-1}	.00357	55.3			.0347	59.7	.0870	57.2
1.0	.00160	54.9			.0154	62.8	.0394	61.5
3.0	.000923	50.5					.0185	66.3

Table IIb

Fractional Attenuation, $A \equiv |Q_1|/|Q_1|_{\omega=0}$ and Phase Angle ($-\phi$, in Degrees) from Potential Flow Heat Response

ω	Pe=.4		Pe=1.0		Pe=2.0		Pe=4.0	
	A	$-\theta$	A	$-\theta$	A	$-\theta$	A	$-\theta$
1×10^{-3}	.999	2.10	1.0		1.0		1.0	
3×10^{-3}	.987	6.18	1.0	1.08	1.0		1.0	
1×10^{-2}	.898	17.7	.996	3.58	1.0		1.0	
3×10^{-2}	.660	32.6	.968	10.3	.998	3.03	1.0	
1×10^{-1}	.377	45.2	.801	26.0	.975	9.81	.997	3.39
3×10^{-1}	.202	53.0	.519	41.4	.845	24.6	.970	9.97
1.0	.0945	59.3	.265	53.6	.518	44.3	.759	28.5
3.0	.0450	65.2	.131	62.1	.267	55.1	.398	91.5
10.0	.0198	76.5	.0589	75.2	.119	63.4		